

Interface roughness and homogeneous linewidths in quantum wells and superlattices studied by resonant acoustic-phonon Raman scattering

T. Ruf, J. Spitzer, V. F. Sapega,* V. I. Belitsky,* M. Cardona, and K. Ploog†
Max-Planck-Institut für Festkörperforschung, Heisenbergstrasse 1, D-70569 Stuttgart,
Federal Republic of Germany

(Received 26 January 1994; revised manuscript received 9 March 1994)

Acoustic-phonon Raman spectra of GaAs/AlAs superlattices show two characteristic features: *Sharp lines* originate in crystal-momentum conserving backscattering by folded superlattice phonons. A *continuous emission background* with superimposed peaks and dips is observed due to disorder-induced scattering from modes of the whole folded acoustic-phonon dispersion. In this case, neither the crystal-momentum component q_z along q_{\parallel} nor perpendicular to the growth direction is conserved. Even in high-quality samples the amount of disorder is such that both effects appear at the same time. These phenomena allow us to obtain information on growth-related and intrinsic parameters of semiconductor superlattices and multiple quantum wells. Gaps of the folded-phonon dispersion cause intensity anomalies in the background emission. From the ratio of such features at mini-Brillouin-zone boundary gaps, for which only q_z is not conserved, to those at internal gaps, where both q_z and q_{\parallel} can take arbitrary values, the degree of interface roughness and the lateral extent of growth islands are deduced. The resonance behavior of the continuous emission and relative changes of wave-vector conserving folded-phonon to background scattering intensities are analyzed in terms of homogeneous and inhomogeneous broadenings of interband critical points. Changes of the homogeneous linewidth with energy and temperature, as well as electron-phonon interaction constants, are determined.

I. INTRODUCTION

Recent investigations of acoustic-phonon Raman scattering in GaAs/AlAs multiple quantum well (MQW) structures and superlattices (SL's) have revealed disorder-induced continuous emission which occurs in addition to the usually observed folded-phonon doublets in the low-energy range.¹⁻⁷ The Raman intensity of this background continuum shows strong resonances near interband critical points such as those between confined electron and hole states or Landau levels.

Explanations for these effects have been given in terms of disorder and relaxation of crystal-momentum conservation. It has been argued that deviations from the SL periodicity, caused by layer thickness fluctuations or interface roughness, perturb the coherent superposition of scattering contributions from all well layers of a sample, which is responsible for backscattering selection rules and crystal-momentum (q_z) conservation along the growth direction. Within a distribution of confinement energies caused by disorder, individual layers can be selectively excited. This leads to Raman scattering from isolated quantum wells, for which q_z does not need to be conserved. Acoustic phonons from the whole mini-Brillouin zone contribute to the spectrum and an emission continuum occurs.¹⁻⁷ At energies corresponding to gaps of the folded-phonon dispersion pronounced intensity anomalies are found.^{2,6} In higher-order processes, q_{\parallel} , the in-plane crystal-momentum component perpendicular to the growth direction, which is zero in first-order backscattering experiments, may assume nonzero

values. This makes internal gaps of the phonon dispersion observable as additional peaks and dips in the spectrum. While the electronic structure is easily perturbed by disorder, acoustic phonons are less sensitive to compositional fluctuations at the interface and maintain the folded character of their dispersion. Therefore both background emission and folded-phonon doublets are observed simultaneously even in high-quality samples.

Mechanisms leading to continuous emission, the assignment of intensity anomalies to folded-phonon dispersion gaps, and the connection of the specific shape of peaks and dips with the wave-vector dependence of the Raman efficiency have been discussed in previous publications.^{6,7} In this paper we exploit the disorder-induced background and folded-phonon Raman scattering to study growth-related and intrinsic parameters of superlattices and multiple quantum wells. In Sec. II we present results on lateral length scales of growth islands for MQW's and SL's with varying layer thicknesses. In Sec. III we discuss the resonance behavior of the continuous emission and its dependence on homogeneous and inhomogeneous broadenings for short-period superlattices. Results from a wider MQW sample are presented in Sec. IV. The tunability of individual resonances between Landau levels is used for a separate determination of homogeneous and inhomogeneous broadenings. From their temperature dependence acoustic- and optic-phonon contributions to the homogeneous linewidth and electron-phonon interaction parameters are determined. Conclusions of our work are given in Sec. V. In the Appendix we discuss additional contributions to the acoustic-phonon

part of the linewidth which have to be considered in order to obtain agreement between theory and experiment.

II. LENGTH SCALES OF INTERFACE ROUGHNESS

A. Continuous emission: General concepts and theory

The characterization of interface quality in semiconductor microstructures fabricated by molecular-beam epitaxy is important in order to obtain information needed for the optimization of growth processes and device performance. Commonly, roughness is regarded as an islandlike compositional perturbation of otherwise atomically flat interfaces.⁸⁻¹¹ Characteristic quantities of such defects are the lateral extent of growth islands, their height in terms of monolayers or potential fluctuations, and surface coverage density. Most optical studies addressing issues of interface roughness have used photoluminescence techniques. From such investigations a comprehensive description of interface roughness has been deduced.¹² Depending on the extent of roughness perturbations compared to the exciton diameter, samples with *rough interfaces*, *large monolayer-flat regions*, or *pseudosmooth (microrough) interfaces* can be distinguished by their luminescence properties.¹² However, to determine whether excitons localized at growth islands of a certain extension will make an observable contribution to the luminescence intensity, their diffusion constant also has to be considered.¹¹ Following such arguments it has been realized that luminescence and cathodoluminescence imaging experiments are only sensitive to smooth parts of an interface which extend over several micrometers.

We have recently described disorder-induced continuous emission in resonant acoustic-phonon Raman spectra of superlattices, which reflects features of the folded-phonon density of states.^{6,7} In this phenomenon scattering from individual quantum wells, which becomes possible by resonant laser excitation of Raman spectra within an inhomogeneously broadened ensemble of energy levels, plays a crucial role. The two major sources for broadening of electronic states in epitaxially grown superlattices are layer thickness fluctuations between different periods and interface roughness within the layers due to growth islands. While period fluctuations only relax the conservation of q_z and make zone-center and zone-edge dispersion gaps observable as characteristic intensity anomalies (peaks and dips) superimposed on a background, the potential steps associated with growth islands allow phonons with nonzero q_{\parallel} to leave a signature in the spectra via scattering processes which can be described in higher-order perturbation theory. The most significant features of these processes are additional dips due to internal gaps at anticrossings of the longitudinal (LA) and transverse (TA) acoustic-phonon dispersion branches for $q_{\parallel} \neq 0$. Evaluating the phonon dispersion for arbitrary q_{\parallel} and q_z by solving the Christoffel equation

for the superlattice,^{13,14} we find that both the magnitude and the energy of internal gaps depend very sensitively on the in-plane crystal-momentum component q_{\parallel} . The mixing of LA and TA branches at internal gaps also lends some Raman activity to TA modes, which are otherwise not observed in backscattering experiments from (001)-oriented superlattices. The strength of TA-related dips is therefore another indicator for the presence of a nonzero q_{\parallel} crystal-momentum component in the scattering.

Theoretical foundations, including a microscopic description of the disorder-induced Raman processes used to model our experimental findings, have been laid in Ref. 7. Here we emphasize qualitative arguments on the approach for the characterization of interface roughness and lateral extensions of growth islands which emerges from our studies. Comparisons of theory with experiment show that best agreement with the emission background and the shape of the intensity anomalies is obtained for an integration over a whole range of q_{\parallel} . Conceptually this corresponds to taking into account the Fourier transform of the interface roughness potential, i.e., the perturbation caused by a growth island in real space. However, there are two approximations that we have made in order to keep the problem tractable. For scattering of electronic intermediate states by the interface roughness potential, i.e., the step where q_{\parallel} becomes involved, we assume the presence of diluted growth islands which are well separated. This avoids computational and conceptual difficulties due to localization and coherence effects. We expect this assumption to be valid for interfaces in high-quality superlattices. Another approximation has to be made about the specific form of the roughness potential, for which we assume a constant and nonzero Fourier distribution for q_{\parallel} between zero and a maximum value $q_{\parallel,\max}$ and no contributions from larger q_{\parallel} . In real space this corresponds to a $\sin(q_{\parallel}r_{\parallel})/(q_{\parallel}r_{\parallel})$ -type potential with in-plane coordinate r_{\parallel} . We take the separation between the first zeros of this function at $r_{\parallel} = \pm\pi/q_{\parallel,\max}$ as a measure of the lateral extent λ of a growth island.

B. Length scales of growth islands: Experiment

Figure 1 shows an experimental (top trace) and a theoretical (lower trace) resonant Raman spectrum in the acoustic-phonon regime for a (001)-oriented (10/10) monolayer GaAs/AlAs superlattice which we shall denote as sample *B* in the following. Similar spectra for samples with (6.7/6.7) and (16/16) monolayers have been published in Ref. 6. We include them in the present discussion as samples *A* and *C*, respectively. The spectra were taken in backscattering geometry using laser excitation, dispersion of the scattered light by a 0.85 m double monochromator, and conventional single-photon counting techniques. Layer thicknesses of the samples were determined by x-ray diffraction and the energies of the folded-acoustic-phonon doublet lines. The spectrum of sample *A* was measured at a temperature of $T = 77$ K, those of samples *B* and *C* were taken at 10 K. All spectra were excited in resonance with the direct transition between the lowest confined heavy hole and electron sub-

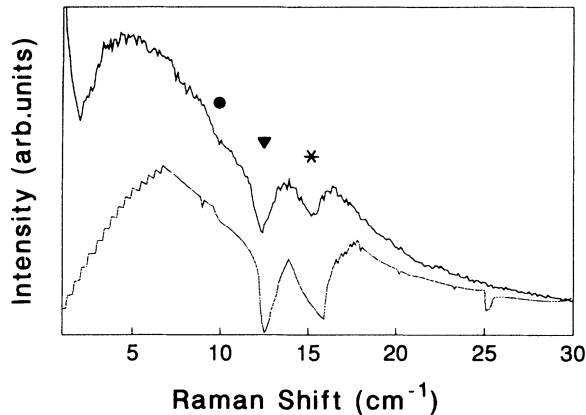


FIG. 1. Experimental (upper traces) and theoretical (lower traces) Stokes-Raman spectra of a (10/10) monolayer GaAs/AlAs superlattice.

bands using parallel polarizations of incident and scattered photons. While the continuous emission and the peaks and dips in the two narrower samples are strong enough to be observed without further efforts, the resonant enhancement of the effect by Landau quantization was exploited for sample *C*.² There the applied field was 11 T and the exciting laser energy was in resonance with the $n=1$ Landau level transition.

Characteristic features of these spectra, such as the continuous emission background, the vanishing scattering intensity for Raman shifts approaching zero, and the specific shape of the intensity anomalies associated with gaps of the folded phonon dispersion, have been discussed in Refs. 2, 6, and 7. Here we focus on the structures from which information on lateral length scales of interface roughness can be obtained. Peaks and dips at the first zone-edge gap of the folded LA phonon dispersion are marked with an asterisk in Fig. 1. Those of the internal gap related to the LA-TA anticrossing are labeled with a filled triangle. The kink at the TA phonon zone edge gap, which becomes Raman active by admixtures of LA modes near the internal gap, is denoted with a filled circle. For vanishing q_{\parallel} , i.e., in the limit of q_{\parallel} -conserving backscattering processes, only peaks and dips at pure LA gaps should be observed. As q_{\parallel} increases, internal gaps (filled triangles) appear with a width depending critically on the in-plane component of crystal momentum. Mode mixing at internal gaps increases with q_{\parallel} , which causes the TA-related kinks (filled circles) to appear. At the same time the energy of the anomalies also increases. For still larger values of q_{\parallel} the LA-TA feature moves up to energies such that it overlaps with the LA anomaly for smaller q_{\parallel} . This causes a smearing out of the characteristic doublet structure and is a clear indication of having chosen too large a value for $q_{\parallel, \max}$.⁶ The theoretical traces in Fig. 1 and in Ref. 6 were obtained by varying $q_{\parallel, \max}$ in a way to obtain the best description of the experimental features. Converting the optimum $q_{\parallel, \max}$ into characteristic lengths λ we obtain $\lambda \approx 150 \text{ \AA}$, 280 \AA , and 450 \AA for samples *A*, *B*, and *C*, respectively, with an estimated error of 20%.

Before drawing further conclusions about interface properties one has to consider that the minimum length scale to which the experiments are sensitive is given by the exciton diameter. Excitons are involved as intermediate electronic states in the Raman process. They are sensitive to potential fluctuations over a range given by the extension of their wave function. With the lateral diameter of confined excitons typically around 250 \AA ,¹¹ we conclude that the value of $\lambda = 150 \text{ \AA}$ for sample *A* is limited by the intrinsic sensitivity of the experimental method. Roughness in this case might extend down to even smaller length scales, but it would not have an influence on the peaks and dips observed in the spectra. The length scales for samples *B* and *C* exceed the experimental sensitivity limit. Within our model we attribute them to lateral extensions of growth islands. These values of λ suggest that interface roughness in our samples exists on microscopic length scales which cannot be accessed by luminescence or cathodoluminescence imaging due to their limitation by exciton diffusion. Indeed, a cathodoluminescence map of the (16/16) monolayer sample does not show any steps due to growth terraces, thus indicating “excellent” interface quality. The same behavior is expected for the other samples where no luminescence satellites from varying confinement energies are observed. The occurrence of features in acoustic-phonon Raman spectra, which are only observable by an in-plane scattering mechanism, indicates that small-scale roughness exists even in high-quality specimens. Raman scattering thus provides access to a quantitative analysis of these effects.

III. CONTINUOUS-EMISSION RESONANCES IN SHORT-PERIOD SUPERLATTICES

A. Theoretical concepts

1. Continuous emission vs folded-phonon doublet scattering

As a consequence of layer thickness fluctuations and interface roughness, acoustic-phonon induced continuous emission spectra of superlattices exhibit pronounced resonances near electronic critical points. Qualitatively this behavior originates in the interplay between *homogeneous linewidths* Γ_{hom} of interband optical transitions, which enter into the expression for the Raman efficiency, and the *inhomogeneous broadening* Γ_{inh} of the distribution of energy levels, over which an integration has to be performed in order to obtain the spectrum of scattered radiation.

Neglecting photon crystal-momentum and zone-folding effects for LA superlattice phonons, i.e., assuming a linear dispersion $\omega(q_z) = vq_z$ for the phonon frequency $\omega(q_z)$ vs superlattice wave vector q_z , with the sound velocity v , the Raman intensity for disorder-induced acoustic-phonon scattering has been demonstrated in Refs. 2 and 5–7 to be given by

$$I[\hbar\omega(q_z)] \propto \sum_{q_z} |M(q_z)|^2 \delta(\hbar\omega_l - \hbar\omega_s \mp \hbar\omega(q_z)) \times \left\{ n[\hbar\omega(q_z)] + \frac{1}{2} \pm \frac{1}{2} \right\} \left| \sum_m e^{iq_z m d} R(m) \right|^2. \quad (1)$$

The delta function ensures energy conservation. Stokes (upper signs) and anti-Stokes (lower signs) emission depend on the Bose-Einstein thermal factor $n[\hbar\omega(q_z)] = 1/\{\exp[\hbar\omega(q_z)/kT] - 1\}$. The matrix element $M(q_z)$ contains details of the deformation-potential interaction of acoustic phonons with confined electronic states of individual quantum wells m with thickness a and is given by

$$M(q_z) = \frac{q_z}{\sqrt{\omega(q_z)}} \frac{\sin \frac{\alpha q_z}{2}}{(\frac{\alpha q_z}{2})} \frac{4N^2}{4N^2 - (\frac{\alpha q_z}{\pi})^2}. \quad (2)$$

The dependence of continuous emission spectra on the electronic subband index N has been demonstrated in Ref. 3. The term $R(m)$ in Eq. (1) contains the resonance denominators of the expression for the Raman scattering amplitude which is given by third-order perturbation theory:

$$R(m) = \frac{1}{[\Delta(m) + i\Gamma_{\text{hom}}][\Delta(m) - \hbar\omega_l + \hbar\omega_s + i\Gamma_{\text{inh}}]}, \quad (3)$$

where $\hbar\omega_l$ and $\hbar\omega_s$ are the energies of incident and scattered photons, respectively, and Γ_{hom} is the half width at half maximum (HWHM) of a Lorentzian line shape which describes the natural broadening of the electronic structure. The detuning parameter $\Delta(m)$ is given by

$$\Delta(m) = \hbar\omega_l - \hbar\omega_{\text{gap}}(m, E_0, N, n, B). \quad (4)$$

$\hbar\omega_{\text{gap}}$ includes all contributions to the critical point energy at which resonance behavior is investigated, i.e., the fundamental gap E_0 , electron and hole confinement in subbands N , and Landau quantization in level n in the case of an applied magnetic field B . Variations of confinement energies due to interface roughness and layer thickness fluctuations are introduced by an explicit dependence of $\hbar\omega_{\text{gap}}$ on the number of the quantum wells m .

The short-period superlattices studied in this section have miniband widths that are small compared to changes in electronic confinement energies by monolayer fluctuations of the well thickness. Their electronic properties are therefore still well described by single quantum well states. Superlattice properties manifest themselves mainly in the backfolding of the acoustic-phonon dispersions. The impact of folded-phonon dispersion gaps on the continuous emission spectra has been discussed in Sec. II. The linear acoustic-phonon dispersion used in the derivation of Eq. (1) is a sufficient approximation for the investigation of resonance effects; intensity anomalies at dispersion gaps shall be neglected in the following.

According to Eq. (1) the Raman intensity for superlattices is obtained by a coherent summation over all individual wells m of the sample. The absolute value of all contributions may only be taken after adding up real and imaginary parts of all the terms. In *ideal structures* electronic confinement energies for all wells are identical. Therefore $R(m)$ does not depend on the layer index m and can be taken out of the sum in Eq. (1). For an infinite number of layers the remaining summation over exponentials ensures crystal-momentum conservation. Thus only sharp folded-phonon lines with $q_z = n2\pi/d$, $n = 0, \pm 1, \pm 2, \dots$, appear in the spectrum. The superlattice period is denoted by d . The generalization to finite light wave vectors k_l and the characteristic doublets is straightforward. In *real structures* disorder causes a distribution of confinement energies. Consequently the resonance factor $R(m)$ varies from layer to layer and cannot be taken out of the sum in Eq. (1) any longer. This causes a partial breakdown of crystal-momentum conservation and continuous emission appears. At each Raman shift the most prominent contribution to the scattering intensity is obtained from those parts of the sample where resonance conditions according to Eq. (3) are fulfilled, i.e., where either incident or scattered photon energies coincide with a particular gap within the distribution. The disorder-induced variation of quantum well energies in real superlattices can be modeled by a Gaussian with an inhomogeneous width Γ_{inh} centered around an average critical point energy E_{gap} . Continuous emission spectra are thus obtained by averaging Eq. (1) over this distribution. This procedure has been carried out in Ref. 5 and the background intensity per unit energy interval is found to be

$$I_B \propto (\langle |R|^2 \rangle - |\langle R \rangle|^2) / \left(\frac{2\pi}{d} v \right). \quad (5)$$

The intensity of crystal-momentum conserving scattering by folded phonons is given by

$$I_F \propto |\langle R \rangle|^2 \delta(\hbar\omega - \hbar\omega(q_z)). \quad (6)$$

In these equations the angular brackets indicate averaging over a Gaussian distribution of HWHM Γ_{inh} . The energy gap fluctuations enter via R as given by Eq. (3). While I_B is nonzero at all Raman shifts, energy and crystal-momentum conservation have to be taken into account in the evaluation of I_F . Equation (6) therefore only yields nonvanishing results for wave vectors $q_z = n2\pi/d + 2k_l$, i.e., at the folded-phonon doublets. The total Raman intensity of Eq. (1) is the sum of I_B and I_F .⁵

From these arguments we find that continuous emission spectra of superlattices are mainly influenced by three parameters: the *homogeneous linewidth* Γ_{hom} , entering via the resonance denominators of the Raman efficiency, the *inhomogeneous broadening* Γ_{inh} of the energy level distribution due to disorder, and the *detuning* Δ of the exciting laser photons with respect to the critical point.

2. Modeling of resonant continuous emission spectra

For off-resonance excitation ($|\Delta| \gg \Gamma_{\text{inh}}$) the Raman spectrum in the acoustic-phonon regime is dominated by contributions from the energy levels near the center of the Gaussian distribution. Even though the levels around the exciting laser energy lead to an enhancement of the Raman signal in incoming or outgoing resonance channels, their contributions are exponentially suppressed since they are located in the tails of the Gaussian distribution. In this case the continuous emission spectrum is determined by the well thickness of the superlattice and by the phonon population factors for Stokes and anti-Stokes scattering, i.e., the sample temperature. The spectrum is characterized by the position of the emission maximum and the width of the intensity distribution. The homogeneous linewidth Γ_{hom} has no influence on its shape. The occurrence of a maximum in the emission spectrum follows from the energy dependence of the electron-phonon matrix element given in Eq. (2). While the Raman intensity decreases for larger energies due to the term $\sin(aq_z/2)/(aq_z/2)$ in $M(q_z)$, a linear increase due to the first term in Eq. (2) determines the spectrum for small Raman shifts. Hence a maximum is found in the intermediate regime. The spectrum is further influenced by the Bose-Einstein statistical factor. For phonon energies that are small compared to the sample temperature [$\omega(q_z) \ll kT$] and Stokes emission, an additional term proportional to $[1 + kT/\omega(q_z)]$ prevents the scattering intensity from reaching zero for vanishing $\omega(q_z)$. For large Raman shifts an additional suppression of the scattering intensity proportional to q_z^{-4} arises from the term which depends on the subband index N in Eq. (2).

Spectra excited in resonance, i.e., $|\Delta| < \Gamma_{\text{inh}}$, show different behavior. For all Raman shifts strong incoming and outgoing resonances with energy levels from the

Gaussian distribution are possible. Near E_{gap} the exponential attenuation of individual resonance contributions by the Gaussian weight factor becomes negligible. Typical acoustic-phonon energies are comparable to the homogeneous linewidth Γ_{hom} . This causes an almost doubly resonant situation, where both energy denominators in Eq. (3) vanish simultaneously, and leads to further enhancement of the scattering intensity. All these effects lead to a shift of the intensity maximum towards the laser line and to a sharpening of the width of the emission continuum as compared to the case of off-resonance excitation.

Figure 2 gives an illustration of these arguments. Continuous emission spectra have been calculated according to the above expressions for a single GaAs quantum well. Figure 2(a) shows spectra for various detunings Δ with respect to a single homogeneously broadened critical point E_{gap} . For large Δ the same spectra are obtained on either side of the resonance. With increasing well width the off-resonance intensity maximum moves towards smaller Raman shifts and vice versa. Near resonance pronounced changes in the position of the maximum intensity and the width of the spectra occur. Incoming resonance causes a prominent peak which moves linearly with Δ . Figure 2(b) shows the same spectra calculated with E_{gap} inhomogeneously broadened, thus modeling a real (imperfect) structure by a disorder-induced variation of single-quantum well confinement energies. While the off-resonance spectra are not changed much compared to those in Fig. 2(a), the inclusion of inhomogeneous broadening leads to a shift of the intensity maximum towards the laser energy and to a sharpening of the spectra over a wide range of detunings around $\Delta = 0$. The analysis of acoustic-phonon continuous emission spectra along these lines thus allows us to obtain information about homogeneous and inhomogeneous widths of the electronic structure in SL's and MQW's.

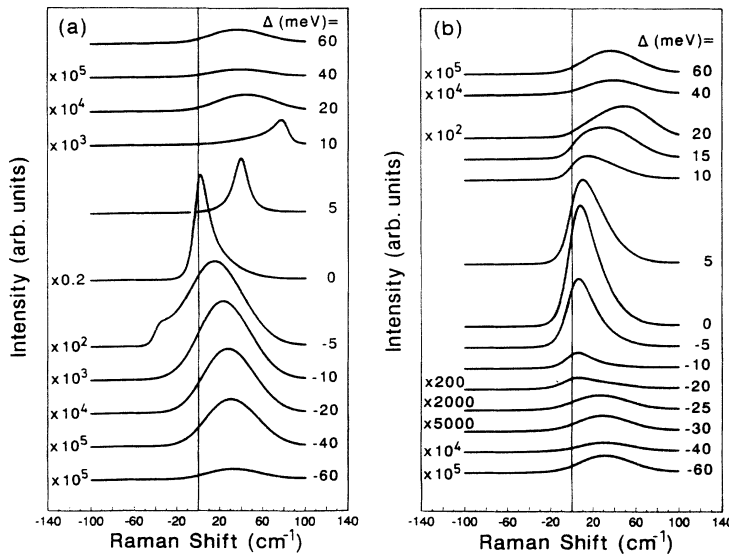


FIG. 2. Acoustic-phonon continuous emission spectra calculated for a single 10 monolayer GaAs quantum well using various detunings from resonance Δ . (a) Calculations for a single homogeneously broadened transition with $\Gamma_{\text{hom}} = 1$ meV at $T = 10$ K. (b) Spectra obtained when inhomogeneous broadening by $\Gamma_{\text{inh}} = 5$ meV is taken into account. Scaling factors with which the respective spectra have been multiplied are given on the left-hand side of each panel; values of Δ in meV are indicated on the right-hand side of each spectrum. Positive Raman shifts indicate Stokes scattering, negative ones anti-Stokes emission.

B. Experiment and discussion

In the short-period superlattices investigated here, layer thickness fluctuations and interface roughness cause such strong continuous emission that folded phonon lines can hardly be detected under resonant excitation. We show in this section that the energy and temperature dependence of Γ_{hom} can be determined experimentally from continuous emission Raman spectra provided that Γ_{inh} is obtained by another method, e.g., from luminescence linewidths.

Figure 3 shows continuous emission spectra of a (10/10) monolayer GaAs/AlAs superlattice for various detunings Δ with respect to the direct Γ - Γ transition between the lowest confined conduction and the highest valence states at the center of the Brillouin zone. The spectra have been taken at a temperature of $T = 16$ K. Points near the laser line where sufficient stray light rejection by the experimental setup was not possible have been omitted. Luminescence spectra show emission associated with this critical point at 1.825 eV. An inhomogeneous width of $\Gamma_{\text{inh}} = 15$ meV is obtained. The lower-lying indirect Γ - X transition from the GaAs valence band to the AlAs X minimum gives luminescence at 1.764 eV. These values are in good agreement with previous determinations.¹⁵ A

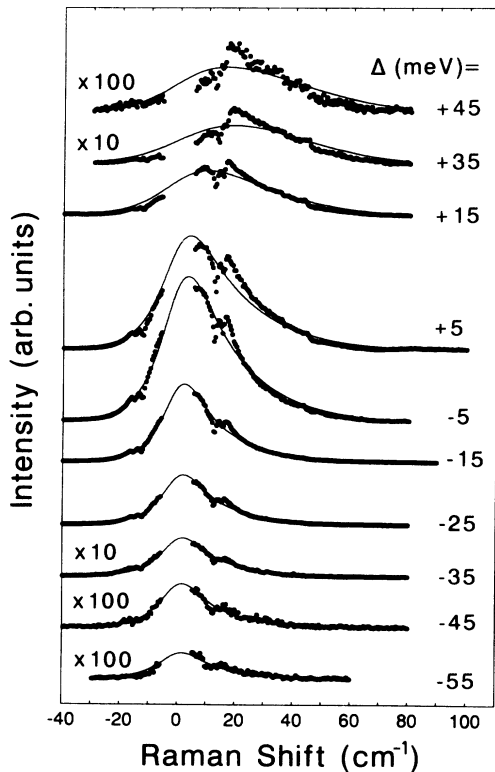


FIG. 3. Experimental (dots) and fitted theoretical (solid lines) continuous emission spectra of a (10/10) monolayer GaAs/AlAs superlattice for various resonance detunings Δ . Fits have been obtained with Γ_{hom} and a linear scaling factor as the only adjustable parameters. A linear background describing the underlying luminescence has been removed from the spectra before fitting. Positive Raman shifts indicate Stokes scattering, negative ones anti-Stokes emission.

maximum in the continuous emission intensity is found for a laser energy larger than that of the Γ - Γ luminescence by about 15 meV. This discrepancy is similar to the frequency shift observed between luminescence excitation and luminescence spectra which can be attributed to the localization of excitonic states.⁸ It has been established that the true absorption edge is located at this higher energy,⁸ which we consequently choose to define zero detuning $\Delta = 0$. These values of Δ are given on the right-hand side of each spectrum in Fig. 3. On the left-hand side of the spectra magnification factors are given where necessary. Around Raman shifts of 15 and 45 cm^{-1} the spectra show intensity anomalies, which have been discussed in Sec. II. For the present investigation of the shape of the continuous emission spectra a bulklike linear acoustic-phonon dispersion has been assumed. Only fluctuations in layer thickness along the growth direction have been considered; in-plane scattering by interface roughness has been neglected. Theoretical spectra calculated under these assumptions therefore do not exhibit any features related to gaps of the folded-phonon dispersion. The solid lines in Fig. 3 are fits to the experimental spectra (dots). They have been obtained using only the homogeneous linewidth Γ_{hom} and a linear scaling factor as adjustable parameters. For Γ_{inh} we have used the value obtained from the luminescence spectrum. The intensity maxima of spectra excited with negative detunings are located close to zero Raman shift. For increasing positive Δ the emission maxima move towards larger shifts on the Stokes side of the spectra. At the same time their width increases.

1. Homogeneous linewidths and Γ - X transfer

The fitted values of Γ_{hom} obtained for the various detunings are shown in Fig. 4. For excitation below resonance the broadening is constant. From the results for

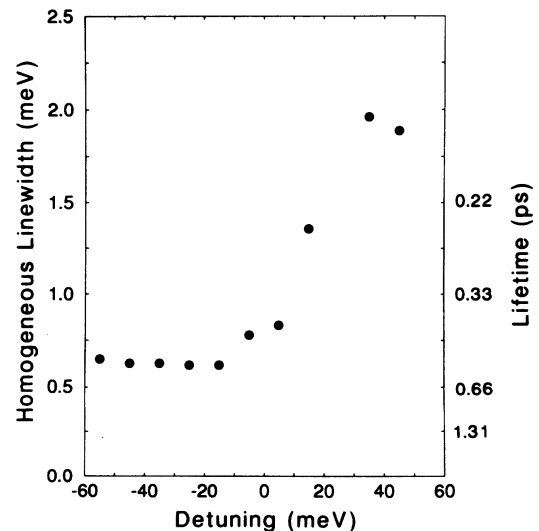


FIG. 4. Homogeneous linewidths Γ_{hom} for different energy detunings Δ obtained from fits of the spectra in Fig. 3.

$\Delta < -10$ meV a value of $\Gamma_{\text{hom}} = (0.63 \pm 0.1)$ meV is obtained. Γ_{hom} increases significantly for positive detunings. This behavior reflects the increasing number of relaxation channels for electrons excited into higher-lying band states of the superlattice dispersion both along and perpendicular to the growth direction. Consequently electronic states with larger Γ_{hom} contribute to the resonant enhancement of the Raman efficiency. Scattering events for laser excitation below the critical point ($|\Delta| \gg \Gamma_{\text{inh}}$) are mediated by virtual processes via direct quantum well electronic transitions. We thus interpret the constant value of Γ_{hom} for negative Δ as the broadening of an average Γ - Γ transition in our sample. In indirect-gap superlattices, such as the $(\text{GaAs})_n/(\text{AlAs})_n$ series for $n < 12$,¹⁶ the broadening of this transition is determined by the transfer time of carriers at the Γ point into the lower-lying X states and does not depend on temperature.¹⁷ Keeping in mind that the value of Γ_{hom} entering the above expressions for the Raman efficiency presents the HWHM of a Lorentzian line shape and defining the lifetime via the $1/e$ decay of the electric field intensity¹⁸ the values of Γ_{hom} can be translated into lifetimes according to $\tau = 0.66/(2\Gamma_{\text{hom}})$ ps, where Γ_{hom} is the experimentally determined HWHM in meV. For the (10/10) monolayer GaAs/AlAs superlattice studied here we find a Γ - X transfer time of $\tau = (524 \pm 90)$ fs. This value compares very favorably with the average transfer time $\tau = (453 \pm 50)$ fs determined for a series of superlattices with about 10 monolayer GaAs well width and varying AlAs barrier thicknesses by energy- and time-resolved differential transmission measurements in Ref. 17. In this work it was also noticed that transfer rates increase for nonresonant excitation above the average direct transition where hot carriers are being created. This effect was attributed to the increasing delocalization of Γ and X envelope functions for energies larger than the Γ - Γ transition.¹⁷ Another contribution to Γ_{hom} arises from the electron-polar optical-phonon interaction, which is responsible for intraband carrier relaxation. In hot-electron luminescence experiments the corresponding scattering time was determined for wider (direct gap)

quantum wells to be about 150 fs.^{19,20} It therefore compares well to measured Γ - X transfer times.¹⁷ Analyzing our results from Fig. 4 with respect to theoretical predictions of carrier relaxation by these two mechanisms should allow a detailed study of their relative importance in short-period superlattices.

In order to further illustrate the influence of homogeneous and inhomogeneous broadenings on resonant acoustic-phonon emission spectra, Fig. 5 summarizes the changes of characteristic quantities of the spectra with Δ and gives a comparison with the theoretically expected behavior. Filled circles connected by a solid line represent values obtained from the fits to the data shown in Fig. 3. Figures 5(a) and 5(b) illustrate the above qualitative arguments. For off-resonance excitation the theoretical intensity maximum is significantly Stokes shifted from the exciting laser line to a position independent of Γ_{hom} . The same holds for the spectral full width at half maximum (FWHM) shown in Fig. 5(b). Approaching resonance from either side, a characteristic crossover to the region where the influence of Γ_{hom} is significant occurs. Spectra excited near resonance show a strong shift of the intensity maximum towards the laser energy and their FWHM is reduced. These changes are more pronounced for small homogeneous linewidths and decrease with increasing Γ_{hom} . Figure 5(c) reflects the decrease of the Raman efficiency with increasing Γ_{hom} according to the resonance denominators given in Eq. (3). For negative Δ the parameters determined from fits to the experiment agree closely with the model calculations. Due to strong overlap with Γ - X luminescence, the crossover region for $\Delta \ll 0$ could not be investigated. For positive detunings the parameters in Figs. 5(a) and 5(b) increase at much smaller Δ than expected. Their changes reflect the increase of Γ_{hom} for energies above the Γ - Γ transition as given in Fig. 4. The maximum intensity of the spectra, given in Fig. 5(c), does not show variations with Γ_{hom} as pronounced as the other two parameters, even though a decrease due to increasing values of Γ_{hom} for positive Δ is noticeable. We attribute this to the higher uncertainty with which scattering intensities for subsequent spectra

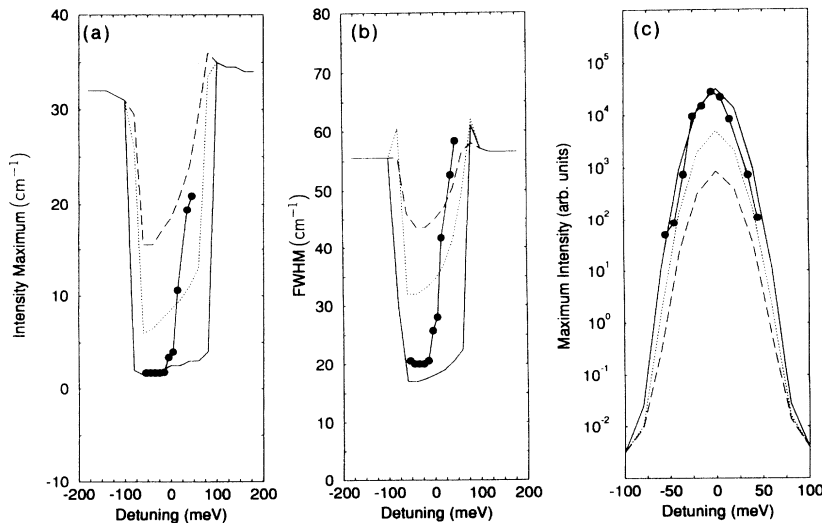


FIG. 5. Characteristic parameters of continuous emission spectra from the superlattice of Fig. 3 with varying detuning Δ compared to model calculations with different Γ_{hom} . (a) Spectral position of the intensity maximum. (b) Spectral full width at half maximum. (c) Maximum Raman intensity. Filled circles connected by a solid line indicate experimental results. Solid, dotted, and dashed lines have been calculated at $T = 10$ K with $\Gamma_{\text{inh}} = 15$ meV and $\Gamma_{\text{hom}} = 0.5, 1, \text{ and } 2$ meV.

can be determined as compared to the more intrinsic parameters of Figs. 5(a) and 5(b).

Experiments have also been performed for the (6.7/6.7) monolayer GaAs/AlAs superlattice of Ref. 6. At $T = 15$ K and $\Delta \simeq 0$ a value of $\Gamma_{\text{hom}} = (1.6 \pm 0.1)$ meV has been obtained from fits to emission continuum spectra. This corresponds to a Γ - X transfer time of about 200 fs. Resonance studies for larger detunings from the Γ - Γ transition in this sample are more complicated due to a strong luminescence background at low temperatures.

2. Electron-phonon interaction in short-period SL's

The possibility to determine homogeneous broadenings even from electronic resonances with considerable inhomogeneous linewidths opens a way to address the question of electron-phonon interaction in reduced dimensions. While this issue will be discussed in detail in the following section, results concerning short-period superlattices shall be presented at this point. Figure 6 shows continuous emission spectra for the (10/10) monolayer GaAs/AlAs sample measured at $\Delta = 0$ for various temperatures. Experimental data (dots) have been fitted with the above model (solid lines) using $\Gamma_{\text{inh}} = 15$ meV. Attributing the origin of inhomogeneous broadening to layer thickness fluctuations and interface roughness, Γ_{inh}

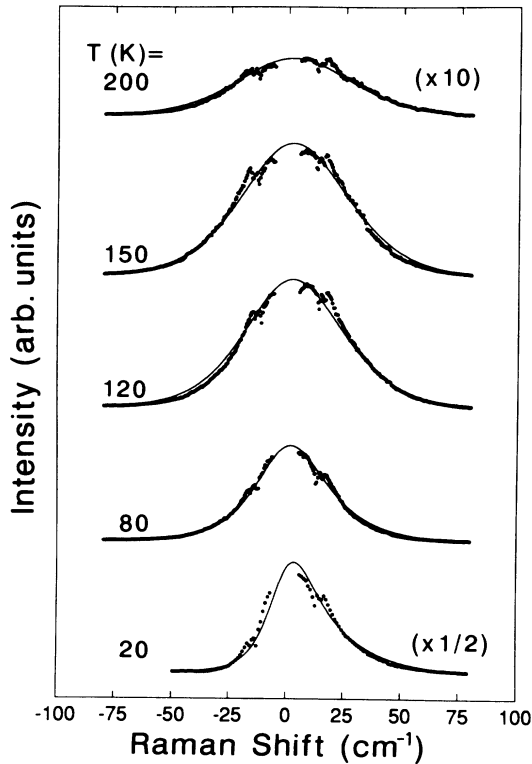


FIG. 6. Experimental Raman spectra (dots) and theoretical fits (solid lines) of the (10/10) monolayer GaAs/AlAs superlattice at various temperatures. Intensity scaling factors are given on the right-hand side of the spectra. Positive Raman shifts indicate Stokes scattering, negative ones anti-Stokes emission.

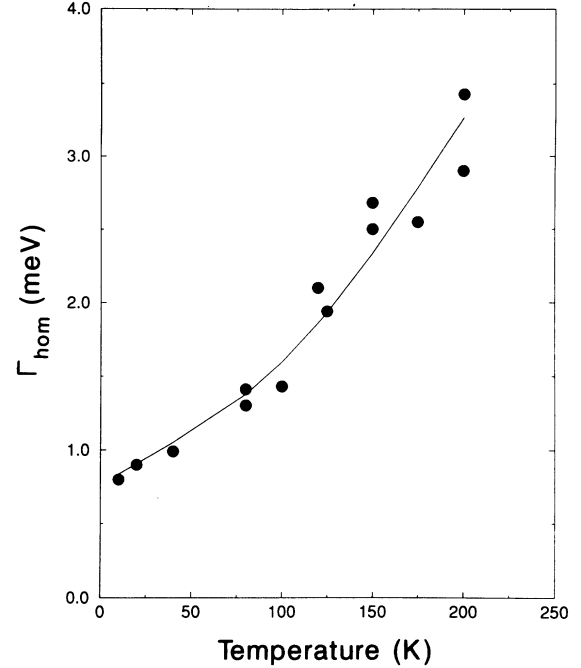


FIG. 7. Temperature dependence of Γ_{hom} obtained from the fits in Fig. 6. Dots give experimental results. The solid line is a fit using acoustic- and optic-phonon contributions to the linewidth.

can be assumed to be temperature independent. With increasing temperature the spectra broaden and their maximum intensity decreases. This decrease indicates an increase of Γ_{hom} . The expected shift of the intensity maximum and the increase of the FWHM with increasing homogeneous broadening are however partially masked by the temperature-induced increase of the Raman signal on the anti-Stokes side of the spectra (see Fig. 5). Homogeneous linewidths obtained from the fits in Fig. 6 are shown in Fig. 7. The solid line is a fit to the data (dots), which include acoustic- and optic-phonon contributions to the linewidth. We find

$$\Gamma_{\text{hom}}(T) = 0.82 \text{ meV} + 6.5 \frac{\mu\text{eV}}{\text{K}} T + \frac{8 \text{ meV}}{e^{\frac{36.7 \text{ meV}}{kT}} - 1}. \quad (7)$$

In fitting this expression to the data, only the constant term and the acoustic-phonon contribution linear in temperature have been varied. The constant term is mostly due to Γ - X transfer. It was found to be independent of temperature in GaAs/AlAs superlattices with scattering processes mediated by the interface-mixing potential (Γ - X_z) and interface roughness (Γ - $X_{x,y}$).¹⁷ The last term represents the longitudinal optic-phonon contribution, characterized by a coupling constant $\Gamma_{ep} = 8$ meV, the use of which will be justified in the next section, and the Bose-Einstein population factor.

IV. HOMOGENEOUS LINEWIDTHS AND ELECTRON-PHONON INTERACTION IN MQW

Homogeneous linewidths have been determined in the preceding section solely from parameters of the continu-

ous emission spectra, such as their width, energy of the maximum, or scattering intensity, under different resonance conditions or temperatures. There we have assumed that crystal-momentum conservation for Raman processes is relaxed to such an extent that coherent effects can be neglected. The validity of this assumption can be checked in Figs. 3 and 6 where almost no acoustic-phonon doublets are observable. Here we demonstrate that both Γ_{hom} and Γ_{inh} can be determined experimentally in samples with an amount of disorder such that the intensities of crystal-momentum conserving folded-phonon scattering and the background emission can be measured separately.

A. Separate determination of Γ_{hom} and Γ_{inh}

As pointed out in Ref. 5, the ratio of folded-phonon doublet scattering and continuous emission is determined by the homogeneous and inhomogeneous broadenings of the underlying electronic structure. This becomes evident in the expressions for the respective Raman intensities I_B and I_F given by Eqs. (5) and (6). In these expressions Γ_{hom} enters via the resonance denominators R . Γ_{inh} comes into play when averaging over a Gaussian distribution of confinement energies.

Figure 8 shows continuous emission spectra of a (16/16) monolayer GaAs/AlAs MQW sample for different magnetic fields. This specimen is the sample C discussed in Sec. II.⁶ We have used the pronounced

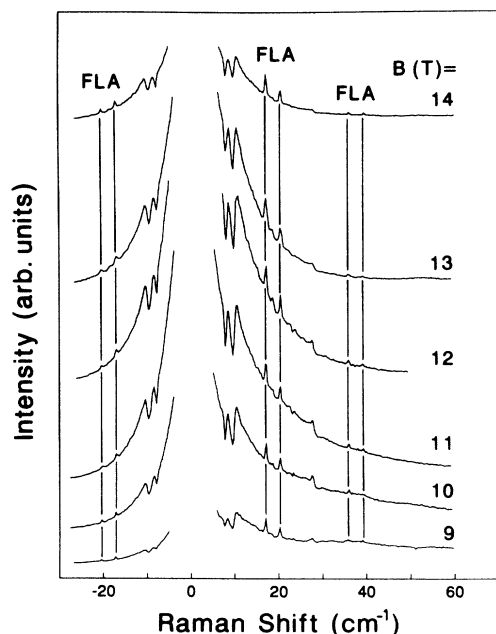


FIG. 8. Resonant acoustic-phonon Raman spectra of a (16/16) monolayer GaAs/AlAs MQW. Folded-phonon lines (marked FLA) and continuous emission are observed simultaneously. Spectra at different magnetic fields correspond to various detunings Δ with respect to the $n=1$ heavy hole electron Landau level transition. $\Delta = 0$ corresponds to 11 T. Positive Raman shifts indicate Stokes scattering, negative ones anti-Stokes emission.

magneto-oscillations of the Raman intensity at interband transitions between Landau levels to obtain sharp resonances. The spectra were measured at 10 K in parallel circular polarizations $\bar{z}(\sigma^-, \sigma^-)z$ and excited with a laser energy of 1.727 eV. Resonance with the $n = 1$ heavy hole to electron Landau level transition occurs at $B_0 = 11$ T. The slope of this transition is $\beta_1 = 2.5$ meV/T. For magnetic fields larger than 9 T the separation of neighboring transitions from the $n = 1$ line exceeds 20 meV. From a luminescence linewidth measurement we find $\Gamma_{\text{inh}} = 3.3$ meV, which is much less than that separation. A magnetic field thus allows one to prepare individual sharp resonances with easily tunable energy mismatch $\Delta(B) = \beta_1(B_0 - B)$. In some cases a background occurs that has been defined and subtracted in the following analysis by connecting the intensities measured at the largest Stokes and anti-Stokes Raman shifts by straight lines. The spectra of Fig. 8 show continuous emission and folded-phonon doublets superimposed on each other. The first LA doublet is found at Raman shifts of 17.1 and 20.5 cm^{-1} . For the largest detunings the continuous emission intensity at the LA doublet is about the same as that of the crystal-momentum conserving signal. In resonance I_B exceeds I_F by up to four times.

The variation of I_B/I_F with magnetic field for the two LA phonons of Fig. 8 is shown in Fig. 9. The solid lines are fitted intensity ratios using Eqs. (5) and (6). Best agreement of theory and experiment was sought using a nonlinear least-squares procedure to optimize Γ_{hom} and Γ_{inh} as the only adjustable parameters. For the 17.1 cm^{-1} mode [Fig. 9(a)] we find values of $\Gamma_{\text{hom}} = 0.64$ meV and $\Gamma_{\text{inh}} = 2.2$ meV. The resonance profile of the 20.5 cm^{-1} mode [Fig. 9(b)] is best described by

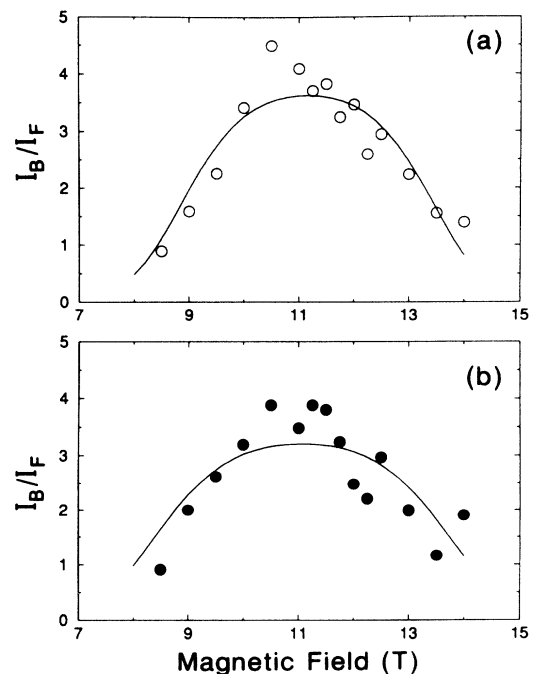


FIG. 9. Resonance behavior of the continuous-emission to folded-phonon scattering intensity ratio for the two modes of Fig. 8 at (a) 17.1 and (b) 20.5 cm^{-1} . The solid lines are fits to the data.

$\Gamma_{\text{hom}} = 0.76 \text{ meV}$ and $\Gamma_{\text{inh}} = 2.5 \text{ meV}$. From calculations with slightly different parameters we estimate an error of $\pm 0.2 \text{ meV}$.

The maximum ratio and the FWHM of the resonances shown in Fig. 9 contain sufficient information for an independent determination of Γ_{hom} and Γ_{inh} . The ratio I_B/I_F increases with increasing $\Gamma_{\text{inh}}/\Gamma_{\text{hom}}$ and vice versa. This reflects the origin of the continuous emission in Raman scattering from individual quantum wells. Smaller values of Γ_{hom} cause sharper electronic resonances, which increase the continuum signal. For larger inhomogeneous widths Γ_{inh} more transitions within the Gaussian distribution contribute significantly to the continuous emission intensity, which is consequently increased. While both broadenings have an influence on the maximum ratio of I_B/I_F , the width of the resonance is only affected by Γ_{inh} . The dependence of I_B/I_F on $\Gamma_{\text{inh}}/\Gamma_{\text{hom}}$ is also highlighted by the results for short-period superlattices in Sec. III. Due to the larger influence of monolayer fluctuations Γ_{inh} increases significantly for smaller well thicknesses. This causes the continuous emission in Figs. 3 and 6 to be much stronger than I_F , the latter being hardly noticeable. Away from resonance, fluctuations in the confinement energies can be neglected with respect to the detuning of the exciting laser from the average transition energy. In this case changes of the resonance denominator R given by Eq. (4) within Γ_{inh} are unimportant and the coherent superposition of scattering contributions in Eq. (1) is reestablished. Continuous emission disappears and Raman spectra are dominated by crystal-momentum conserving folded-phonon scattering (LA doublets). At this point the application of high magnetic fields is particularly useful. The short-period superlattices investigated in Sec. III are indirect, their main luminescence signal occurs at the lower-lying Γ - X transition, and the resonance behavior near the Γ - Γ energy can be easily studied. In wider quantum wells, such as the sample studied here, strong luminescence at the direct transition prohibits the observation of Raman scattering in the absence of a magnetic field. In its presence, a series of strong resonances occurs at energies away from the luminescence background due to Landau quantization and detailed studies become possible.

B. Temperature dependence of Γ_{hom}

The dependence of the intensity ratio I_B/I_F on Γ_{hom} and Γ_{inh} and its resonance behavior constitutes a connection of these fundamental electronic structure parameters to experimental quantities. Figure 10 shows a series of Raman spectra from the (16/16) monolayer GaAs/AlAs sample measured at various temperatures. All spectra have been obtained with zero detuning Δ . To compensate temperature shifts of the electronic structure, the spectra have been taken with varying excitation energies such that resonance with the above $n=1$ Landau level transition always occurs near $B=11 \text{ T}$. This has been checked by monitoring the magneto-oscillations of the continuous emission intensity close to the laser line in each case.² While the overall scattering intensity of

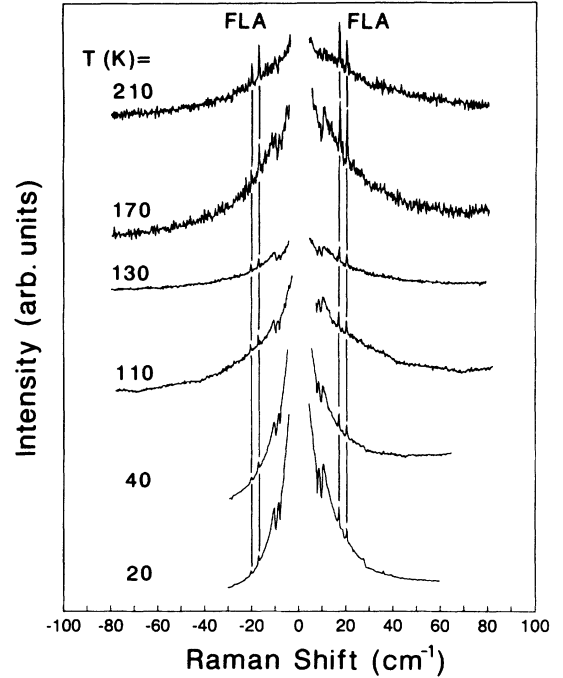


FIG. 10. Temperature-dependent acoustic-phonon Raman spectra of the (16/16) monolayer GaAs/AlAs MQW. Folded-phonon doublets are marked FLA. Positive Raman shifts indicate Stokes scattering, negative ones anti-Stokes emission.

the spectra decreases with increasing temperature, characteristic changes in the relative intensities of continuous emission and folded-phonon scattering are found. As I_B/I_F decreases with increasing temperature, the folded-phonon lines emerge from the background signal. Attributing the origin of Γ_{inh} to layer thickness fluctuations and interface roughness, the inhomogeneous linewidth can be assumed to be independent of temperature. With the above values of Γ_{inh} determined from the low-temperature resonance behavior, changes of I_B/I_F with temperature can be translated into a temperature dependence of Γ_{hom} . Figure 11 shows values of $\Gamma_{\text{hom}}(T)$ determined this way.

C. Electron-phonon interaction in MQW

In bulk semiconductors as well as quantum wells and superlattices the most important contributions to the temperature dependence of Γ_{hom} are due to electron-phonon interaction.²¹⁻²⁶ Generally, deformation-potential and piezoelectric scattering mechanisms are considered for the interaction of the lowest exciton state with *acoustic phonons*. This leads to a linear increase of Γ_{hom} with temperature. Fröhlich coupling is invoked for scattering with *longitudinal optic phonons*. In this case the linewidth is proportional to the Bose-Einstein population factor $n_{\text{LO}}(T)$. Scattering by *ionized impurities* gives an additional thermal-activation type contribution to $\Gamma_{\text{hom}}(T)$, which shall not be considered

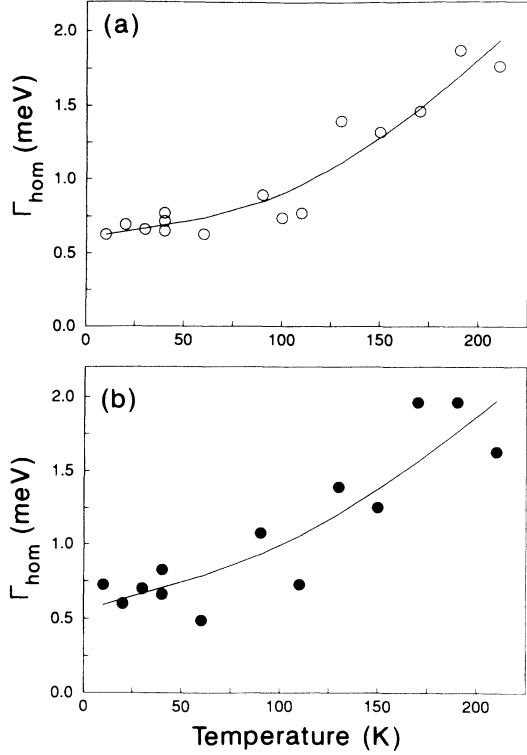


FIG. 11. Temperature dependence of the homogeneous linewidth Γ_{hom} for the sample of Fig. 10 determined from the resonance intensity ratio I_B/I_F . The solid lines are fits of a theoretical model for $\Gamma_{\text{hom}}(T)$. A separate analysis has been performed for (a) the 17.1 cm^{-1} and (b) the 20.5 cm^{-1} phonon.

here. The change of the homogeneous linewidth with temperature is thus given by

$$\Gamma_{\text{hom}}(T) = \Gamma_0 + \sigma T + \Gamma_{ep} n_{\text{LO}}(T). \quad (8)$$

The parameters in this expression have been subject to intense theoretical^{23–26} and experimental investigations. A majority of experiments are based either on the determination of spectral linewidths or on the study of time-domain phenomena. Modulation spectroscopy, especially photoreflectivity, and absorption measurements have been performed to study the width of direct transi-

tions in bulk materials and quantum wells.^{27–31} Luminescence linewidths have been analyzed in terms of $\Gamma_{\text{hom}}(T)$ and Γ_{inh} and attempts to deconvolute the two parameters have been made.^{25,32–34} The development of the time-resolved four wave mixing technique and energy- and time-resolved differential transmission experiments have allowed a direct measurement of exciton dephasing times which are related to Γ_{hom} .^{35–37} Tables I and II summarize experimental values of σ and Γ_{ep} for bulk GaAs and GaAs/ $\text{Al}_x\text{Ga}_{1-x}\text{As}$ quantum wells obtained by various techniques.

The solid lines in Fig. 11 have been obtained by fitting Eq. (8) to the experimental results obtained at the two frequencies. Using an optic-phonon energy of $\hbar\Omega_{\text{LO}} = 36.7 \text{ meV}$ and optimizing the other three parameters we find

$$\Gamma_{\text{hom}}(T) = 0.60 \text{ meV} + 2.1 \frac{\mu\text{eV}}{\text{K}} T + 5.9 \text{ meV} n_{\text{LO}}(T) \quad (9)$$

for the 17.1 cm^{-1} phonon and

$$\Gamma_{\text{hom}}(T) = 0.56 \text{ meV} + 3.7 \frac{\mu\text{eV}}{\text{K}} T + 4.2 \text{ meV} n_{\text{LO}}(T) \quad (10)$$

for the one at 20.5 cm^{-1} . From these fits we determine the constant for the acoustic-phonon contribution linear in T as $\sigma = (3 \pm 1) \mu\text{eV}/\text{K}$ and that of the LO phonon term as $\Gamma_{ep} = (5 \pm 1) \text{ meV}$.

The value found for the acoustic-phonon scattering coefficient σ is in good agreement with other experimental determinations and provides further evidence for a reduction of σ with decreasing well thickness. For bulk GaAs absorption measurements of the exciton linewidth give $\sigma = 12 \mu\text{eV}/\text{K}$.^{23,38} From time-resolved experiments the acoustic-phonon contribution is determined to be $(8.5 \pm 0.5) \mu\text{eV}/\text{K}$.³⁶ In GaAs quantum wells values of $\sigma = 4.5, 2.5,$ and $1.25 \mu\text{eV}/\text{K}$ have been found from dephasing-time measurements for layer thicknesses of 277, 135, and 120 Å, respectively.³⁶ For wells with widths of 150 and 325 Å, acoustic-phonon contributions of $\sigma = 1.7$ and $3 \mu\text{eV}/\text{K}$ have been obtained from linewidth studies.³³ Theoretical predictions of σ for bulk semiconductors deviate significantly from the experimental values. Possible mechanisms that may reconcile the large discrepancy between theory and experiment for bulk GaAs are discussed

TABLE I. Experimental values of the acoustic-phonon scattering coefficient σ contributing to the homogeneous linewidth given by Eq. (8) for bulk GaAs and GaAs/ $\text{Al}_x\text{Ga}_{1-x}\text{As}$ quantum wells with different layer thickness a . See text for a discussion of the various experimental techniques and fitting procedures used in the determination of these constants.

a (Å)	σ ($\mu\text{eV}/\text{K}$)	Technique	Reference
bulk	12	absorption	23, 38
bulk	8.5 ± 0.5	dephasing time	36
325	3	photoluminescence linewidth	33
277	4.5	dephasing time	36
150	1.7	photoluminescence linewidth	33
135	2.5	dephasing time	36
120	1.25	dephasing time	36
45	3 ± 1	Raman	this work

TABLE II. Experimental values of the coefficient Γ_{ep} due to exciton-optic phonon scattering contributing to the homogeneous linewidth given by Eq. (8) for bulk GaAs and GaAs/Al_xGa_{1-x}As quantum wells with different layer thickness a . See text for details on the various experimental techniques and fitting procedures used to determine these constants.

a (Å)	Γ_{ep} (meV)	Technique	Reference
bulk	7	absorption	38
bulk	20 ± 1	photoreflectance	29
205	8.1	photoreflectance	27
200	7.8	absorption	32
200	4.7 ± 0.6	photoreflectance	29, 30
130	3.7 ± 0.5	photoreflectance	29, 30
120	12.3	photoluminescence linewidth	32
102	5.5	absorption	39
96	10.4	absorption	32
84	11.1 ± 1	photoluminescence linewidth	40
80	1.1 ± 0.9	photoreflectance	29, 30
78	12 ± 1	photoluminescence linewidth	40
60	1.7 ± 0.9	photoreflectance	29, 30
60	10.9	absorption	32
53	9.3	reflectance	28
45	5 ± 1	Raman	this work

in the Appendix.

Experimental values for Γ_{ep} in bulk GaAs vary over a wide range between 7 meV (Ref. 38) and 20 meV.²⁹ The same holds for GaAs quantum wells where values between 1.1 meV for layers with 80 Å (Ref. 29) and 10.9 meV for a sample with 60 Å (Ref. 32) have been reported. Similar discrepancies are also found for the dependence of Γ_{ep} on layer thickness. Γ_{ep} is predicted to increase with decreasing well width up to three times, depending on the effective masses, in Ref. 26. Values of Γ_{ep} obtained from a careful deconvolution of Γ_{inh} and Γ_{hom} in Ref. 32 are considered to confirm this notion.²⁶ Other linewidth measurements suggest Γ_{ep} to scale linearly with well thickness and the dependence of the Fröhlich Hamiltonian on the wave vector of confined phonons is invoked to account for the observations.²⁹ It is therefore evident that more experimental efforts and a better theoretical understanding are required in order to resolve these controversies. In view of the highly controversial reduction of Γ_{ep} with layer thickness and its implications on changes of the electron-phonon interaction with dimensionality, a thorough description of the bulk behavior is also called for.

At this point our results from resonant acoustic-phonon Raman scattering may provide a stimulus for a consistent description of these effects. Let us note that most experiments that measure Γ_{ep} have been analyzed neglecting the acoustic-phonon term, linear in temperature.^{27,32,28-30} According to our and the above-mentioned other determinations of $\sigma \simeq 3 \mu\text{eV/K}$ in GaAs quantum wells, this term accounts for a contribution to Γ_{hom} of almost 1 meV at room temperature and therefore cannot be neglected with respect to an optic-phonon induced broadening of 2.5 meV evaluated for $\Gamma_{ep} = 8 \text{ meV}$ and the LO phonon of GaAs. In fact we obtain a value of $\Gamma_{ep} = 8.6 \text{ meV}$ from fitting the data of Fig. 11 with Eq. (8) while setting $\sigma = 0$. Our results for GaAs wells

with a thickness a of 45 Å are thus in good agreement with most other determinations ranging from $a = 53 \text{ Å}$ [$\Gamma_{ep} = 9.3 \text{ meV}$ (Ref. 28)] over 60 Å [$\Gamma_{ep} = 10.9 \text{ meV}$ (Ref. 32)] and 96 Å [$\Gamma_{ep} = 10.4 \text{ meV}$ (Ref. 32)] up to about $a = 200 \text{ Å}$ [$\Gamma_{ep} = 7.8, 8.1 \text{ meV}$ (Refs. 32 and 27)], regarding that the acoustic-phonon contribution has been neglected in these studies.

Much smaller values of Γ_{ep} have been obtained in the photoreflectance study of GaAs quantum wells with thicknesses between $a = 60$ and 200 Å in Refs. 29 and 30. Decreasing coupling constants between $\Gamma_{ep} = 4.7 \text{ meV}$ at $a = 200 \text{ Å}$ and 1.7 meV at $a = 60 \text{ Å}$ have been interpreted as a reduction of the electron-phonon interaction due to phonon confinement and the reduced dimensionality of electronic subbands.^{29,30} In this context we want to emphasize the necessity to treat Γ_{hom} and Γ_{inh} separately when extracting information on coupling constants from linewidth measurements. This requirement is fulfilled in our analysis and has also been met by earlier studies which used a deconvolution of homogeneous and inhomogeneous contributions to the broadening of excitonic transitions.³² It can only be circumvented in highest-quality quantum wells where Γ_{inh} is much smaller than Γ_{hom} .^{27,28,33} In samples with $\Gamma_{inh} \gg \Gamma_{hom}$ the increase of the homogeneous linewidth with T will show up in line-shape fits which do not distinguish between these two quantities, at much higher temperatures, and thus lead to a flatter increase of the broadening vs T . This might lead one to interpret the smaller values obtained for Γ_{ep} from such fits as a reduction of the electron-phonon interaction.^{29,30} In fact we also obtain a significantly reduced value of $\Gamma_{ep} = 2.7 \text{ meV}$ for our sample when fitting Eq. (8) with $\sigma = 0$ to the temperature-dependent width of the continuous emission magneto-oscillation of the $n=1$ heavy hole to electron Landau level

transition under the above conditions, which is essentially determined by Γ_{inh} .

From our and other determinations of Γ_{ep} , which take homogeneous and inhomogeneous broadenings into account or use samples where the influence of Γ_{inh} can indeed be neglected,^{27,32,28,33} it appears that a value of $\Gamma_{ep} \simeq 5$ meV reasonably describes the LO phonon contribution to $\Gamma_{\text{hom}}(T)$ for well widths between 45 and 200 Å, provided that the acoustic-phonon term is taken into account. This limit may even be extendable to well thicknesses below 30 Å as follows from Sec. III and Fig. 7 where a constant $\Gamma_{ep} = 8$ meV has been used for a (10/10) monolayer GaAs/AlAs superlattice and reasonable values for σ and Γ_0 have been obtained from the fit of $\Gamma_{\text{hom}}(T)$ as given by Eq. (7). Reliable theoretical estimates of Γ_{ep} for bulk GaAs and other semiconductors have to take into account a variety of effects, such as excitonic-polariton states, an accurate description of mixed valence bands, or the various contributions to exciton-phonon scattering from discrete and continuum excitons.²³ It is also necessary to treat the excitonic continuum as scattering states; simple plane waves are insufficient.²³ A careful calculation along these lines has recently yielded a value of $\Gamma_{ep} = 8$ meV for bulk GaAs.⁴¹ This value, which is also in agreement with theory and experiment of Ref. 38, is rather close to the Γ_{ep} found for GaAs quantum wells. It resolves the problem of an apparent reduction of the electron-phonon interaction in quantum wells as compared to the bulk posed by the previously evaluated theoretical value of $\Gamma_{ep} \simeq 20$ meV.²³ The experimental coupling constant $\Gamma_{ep} = 20$ meV for bulk GaAs of Refs. 29 and 30 can be reconciled with these lower values of Γ_{ep} by including an acoustic-phonon contribution of $\sigma = 10 \mu\text{eV/K}$, the average of the experimental determinations in Refs. 23, 38, and 36, which reduces Γ_{ep} to about 12 meV. New calculations, which properly consider phonon confinement and changes of the electronic structure with decreasing well thickness, yield that Γ_{ep} is almost independent of well width and hardly different from the bulk value.⁴¹ Small variations of Γ_{ep} by about 1 meV, however, are predicted to occur at layer thicknesses where electronic intersubband energies are comparable to that of the LO phonon.⁴¹ It is for this reason that we have decided to fit the data of Fig. 7 [see Eq. (7)] with the constant $\Gamma_{ep} = 8$ meV obtained from these calculations.⁴¹ Similar results have also been obtained in Ref. 42 using bulk phonons and plane-wave continuum states, but the three-dimensional limit of Γ_{ep} could not be recovered. Further experimental and theoretical work is required to determine the remaining minor differences between bulk and two-dimensional values of Γ_{ep} . These results for Γ_{hom} , a quantity which is only sensitive to the total electron-optic-phonon interaction contributions from all confined and interface phonons, bear no relationship to experiments which distinguish between the individual modes, such as time-resolved intraband Raman scattering.⁴³ There it has been demonstrated that the electron-phonon coupling for confined phonons indeed decreases with well thickness whereas, on the other hand, that for interface modes becomes more significant.

V. CONCLUSIONS

We have used resonant acoustic-phonon Raman scattering to investigate growth-related and intrinsic parameters of GaAs/AlAs quantum wells and superlattices. Disorder due to layer thickness fluctuations and interface roughness is the origin of a relaxation of crystal-momentum conservation in Raman processes. In addition to crystal-momentum conserving folded-phonon doublets, disorder causes a Raman emission continuum where all acoustic phonons from the mini-Brillouin zone contribute to the scattering. The continuum reflects features of the phonon density of states, such as dispersion gaps of the longitudinal branches at $q_z = 0$ and π/d , but also at internal gaps where anticrossings of LA and TA branches occur for $q_{\parallel} \neq 0$. The ratio of features at the zone edge and at internal dispersion gaps has been interpreted in terms of characteristic sizes of growth islands which mediate higher-order Raman processes as in-plane scattering potentials.

Experimental continuous emission spectra have been theoretically modeled. From fits of their resonance and temperature behavior we have obtained values for the homogeneous linewidth of the underlying electronic structure. In indirect gap superlattices this method can be used to determine Γ - X transfer times. It also allows one to determine contributions to the homogeneous linewidth by electron-acoustic-phonon and optic-phonon interaction even in samples with considerable inhomogeneous broadening.

In quantum wells we have used resonances in the ratio of continuous emission and folded-phonon scattering to determine homogeneous and inhomogeneous linewidths separately. We have analyzed the temperature dependence of the homogeneous linewidth for a sample with a well width of 45 Å and found a reduction of the electron-acoustic-phonon interaction contribution to the linewidth as compared to the bulk. Nevertheless this contribution may not be neglected in a thorough analysis of temperature-dependent linewidths. The coupling constant due to electron-optic-phonon interaction is not considerably reduced as compared to bulk GaAs. We have pointed out the importance of treating homogeneous and inhomogeneous linewidths separately in such studies. The failure to do so has been identified as the origin of previous misinterpretations of reduced coupling constants for smaller quantum well thicknesses as strongly suppressed electron-optic phonon interaction.

ACKNOWLEDGMENTS

V.I.B. and V.F.S. thank the Max-Planck-Gesellschaft for financial support and the Max-Planck-Institut für Festkörperforschung for hospitality. Thanks are due to H. Hirt, M. Siemers, and P. Wurster for technical assistance. We would like to thank T. L. Reinecke and J. Kuhl for valuable discussions and a critical reading of the manuscript.

APPENDIX

A comprehensive theoretical investigation of temperature-dependent exciton linewidths in bulk semiconduc-

tors has been given in Ref. 23. The contribution to the linewidth from exciton-acoustic-phonon interaction has been evaluated using the deformation potential and the piezoelectric scattering mechanisms. While piezoelectric coupling was found to give a negligible contribution to the broadening, a coefficient of $\sigma = 0.64 \mu\text{eV/K}$ was obtained for the term linear in temperature due to deformation potential interaction with longitudinal acoustic phonons in bulk GaAs. In view of the large discrepancy of this theoretical result to experimental values of $\sigma = 12 \mu\text{eV/K}$ (Refs. 23 and 38) and $\sigma = (8.5 \pm 0.5) \mu\text{eV/K}$,³⁶ excitonic polariton effects were additionally taken into account in the calculations of Ref. 23. This yields values of $\sigma_T = 0.95 \mu\text{eV/K}$ and $\sigma_L = 1.12 \mu\text{eV/K}$ for the transverse and longitudinal exciton polariton branches, respectively. Even though these coefficients are somewhat larger than the one calculated without this coupling, they are still much smaller than the experimental value. Due to the insufficient understanding of bulk properties similar calculations for MQW's have not been attempted. In this appendix we estimate the influence of two further contributions to σ in bulk GaAs which might be used in a more detailed calculation to overcome the above problem.

One additional contribution to σ is found in a more complete treatment of electron-acoustic-phonon interaction which usually^{23,24} only includes longitudinal acoustic phonons and the hydrostatic component of the deformation potential. The next step beyond this approximation has to take into account also the scattering by longitudinal and transverse acoustic phonons via the shear components of the deformation potential which acts on the valence band states. In order to circumvent the complications brought about by the mixing of the valence bands and the anisotropy of the elastic properties, an effective deformation potential has been defined as⁴⁴

$$\Xi_{\text{eff}}^2 = a_v^2 + \frac{C_l}{C_t} (b_v^2 + \frac{1}{2} d_v^2), \quad (\text{A1})$$

where a_v , b_v , and d_v are the valence band deformation potentials and C_l and C_t are spherically averaged elastic constants of longitudinal and transverse dispersion branches given by

$$C_l = \frac{1}{5} (3C_{11} + 2C_{12} + 4C_{44}), \quad (\text{A2})$$

$$C_t = \frac{1}{5} (C_{11} - C_{12} + 3C_{44}).$$

From the pressure dependence of deep transition metal defects absolute values $a_c = (-9.3 \pm 1) \text{eV}$ and $a_v = (-0.7 \pm 1) \text{eV}$ of hydrostatic conduction and valence band deformation potentials have been determined using a gap

deformation potential of $|a_c - a_v| = 8.6 \text{eV}$.⁴⁵ With these numbers and elastic constants from Ref. 46 an effective valence band deformation potential of $\Xi_{\text{eff}} = 6.1 \text{eV}$ is obtained. Due to the smallness of a_v this value is almost entirely due to the shear components b_v and d_v , which are usually neglected in the calculation of the broadening coefficient σ . Adding to the dependence of σ on the square of the gap deformation potential the valence band contribution approximately equal to Ξ_{eff}^2 increases its value by 50%, almost as much as when excitonic polariton effects are taken into account.

Another contribution to σ has its origin in the fact that typical energies of final states in processes of exciton-acoustic-phonon scattering are much smaller than the broadening caused by other mechanisms. Due to energy and crystal-momentum conservation acoustic phonons absorbed in a scattering event from the bottom of the exciton dispersion have an energy of

$$\bar{E} = \frac{\hbar^2 q^2}{2M} = \hbar v q. \quad (\text{A3})$$

With parameters for GaAs ($M = m_e^* + m_h^* = 0.55 m_0$) and a longitudinal sound velocity of $v = 4.8 \times 10^5 \text{cm/s}$, a value of $\bar{E} \simeq 150 \mu\text{eV}$ is obtained. According to Fermi's golden rule, the scattering rate is proportional to the density of final states at this energy. However, due to other processes, such as electron-optic-phonon interaction and residual broadenings, the actual total homogeneous linewidth Γ_{hom} is much larger than \bar{E} . This leads to a modification of the final density of states, which for bulk semiconductors vanishes at the direct band gap proportional to \sqrt{E} and therefore to an increase of σ . The linewidth then has to be determined in a self-consistent way similar to the approach chosen in Ref. 47. An estimate of the change in σ due to this effect is possible by adding the actual linewidth as an imaginary part to \bar{E} in the expression for the scattering rate which then reads

$$\sigma T \sim \sqrt{\bar{E} + i\Gamma_{\text{hom}}}. \quad (\text{A4})$$

Using an observed broadening of $\Gamma_{\text{hom}} \simeq 2 \text{meV}$ at 100 K (Ref. 38) for bulk GaAs and the above value of \bar{E} , the enhancement factor for the linewidth coefficient σ from acoustic-phonon scattering can be estimated as $\sqrt{2/0.15} = 3.7$.

From these estimates we find a total enhancement of σ by more than a factor of 5 when both effects on the scattering are taken into account. Together with the enhancement by a factor of 2 due to excitonic polariton formation an order of magnitude increase of σ can be justified and good agreement between theory and experiment is obtained. We hope that these suggestions will stimulate further studies and eventually lead to a theoretical description of σ even for MQW's.

* On leave from the A. F. Ioffe Physics-Technical Institute, Russian Academy of Science, 194021 St. Petersburg, Russia.

† Permanent address: Paul-Drude-Institut für Festkörper-

elektronik, Hausvogteiplatz 5-7, D-10117 Berlin, Federal Republic of Germany.

¹ P. S. Kop'ev, D. N. Mirlin, V. F. Sapega, and A. A. Sirenko, Pis'ma Zh. Eksp. Teor. Fiz. **51**, 624 (1990) [Sov. Phys.

- JETP Lett. **51**, 708 (1990)].
- ² V. F. Sapega, V. I. Belitsky, T. Ruf, H. D. Fuchs, M. Cardona, and K. Ploog, Phys. Rev. B **46**, 16005 (1992).
 - ³ V. F. Sapega, V. I. Belitsky, A. J. Shields, T. Ruf, M. Cardona, and K. Ploog, Solid State Commun. **84**, 1039 (1992).
 - ⁴ T. Ruf, V. F. Sapega, J. Spitzer, V. I. Belitsky, M. Cardona, and K. Ploog, in *Phonons in Semiconductor Nanostructures*, Vol. 236 of *NATO Advanced Study Institute, Series E: Applied Sciences*, edited by J. P. Leburton, J. Pascual, and C. Sotomayor Torres (Kluwer, Dordrecht, 1993), p. 83.
 - ⁵ D. N. Mirlin, I. A. Merkulov, V. I. Perel', I. I. Reshina, A. A. Sirenko, and R. Planel, Solid State Commun. **84**, 1093 (1992).
 - ⁶ T. Ruf, V. I. Belitsky, J. Spitzer, V. F. Sapega, M. Cardona, and K. Ploog, Phys. Rev. Lett. **71**, 3035 (1993).
 - ⁷ V. I. Belitsky, T. Ruf, J. Spitzer, and M. Cardona, Phys. Rev. B **49**, 8263 (1994).
 - ⁸ C. Weisbuch, R. Dingle, A. C. Gossard, and W. Wiegmann, Solid State Commun. **38**, 709 (1981).
 - ⁹ D. Paquet, Superlatt. Microstruct. **2**, 429 (1986).
 - ¹⁰ M. Tanaka and H. Sakaki, J. Cryst. Growth **81**, 153 (1987).
 - ¹¹ M. A. Herman, D. Bimberg, and J. Christen, J. Appl. Phys. **70**, R1 (1991).
 - ¹² R. F. Kopf, E. F. Schubert, T. D. Harris, and R. S. Becker, Appl. Phys. Lett. **58**, 631 (1991).
 - ¹³ S. Tamura, D. C. Hurley, and J. P. Wolfe, Phys. Rev. B **38**, 1427 (1988).
 - ¹⁴ B. A. Auld, *Acoustic Fields and Waves in Solids* (Wiley, New York, 1973), Vol. 1, p. 210.
 - ¹⁵ D. J. Mowbray, M. Cardona, and K. Ploog, Phys. Rev. B **43**, 11 815 (1991).
 - ¹⁶ R. Cingolani, K. Ploog, L. Baldassarre, M. Ferrara, M. Lugarà, and C. Moro, Appl. Phys. A **50**, 189 (1990).
 - ¹⁷ J. Feldmann, J. Nunnenkamp, G. Peter, E. O. Göbel, J. Kuhl, K. Ploog, P. Dawson, and C. T. Foxon, Phys. Rev. B **42**, 5809 (1990).
 - ¹⁸ E. Hecht and A. Zajac, *Optics* (Addison-Wesley, Reading, MA, 1974), p. 415.
 - ¹⁹ B. P. Zakharchenya, P. S. Kop'ev, D. N. Mirlin, D. G. Polakov, I. I. Reshina, V. F. Sapega, and A. A. Sirenko, Solid State Commun. **69**, 203 (1990).
 - ²⁰ P. S. Kop'ev, D. N. Mirlin, D. G. Polyakov, I. I. Reshina, V. F. Sapega, and A. A. Sirenko, Fiz. Tekh. Poluprovodn. **24**, 1200 (1990) [Sov. Phys. Semicond. **24**, 757 (1990)].
 - ²¹ P. Lautenschlager, P. B. Allen, and M. Cardona, Phys. Rev. B **33**, 5501 (1986).
 - ²² S. Gopalan, P. Lautenschlager, and M. Cardona, Phys. Rev. B **35**, 5577 (1987).
 - ²³ S. Rudin, T. L. Reinecke, and B. Segall, Phys. Rev. B **42**, 11 218 (1990).
 - ²⁴ T. Takagahara, Phys. Rev. B **31**, 6552 (1985).
 - ²⁵ J. Lee, E. S. Koteles, and M. O. Vassell, Phys. Rev. B **33**, 5512 (1986).
 - ²⁶ S. Rudin and T. L. Reinecke, Phys. Rev. B **41**, 3017 (1990).
 - ²⁷ O. J. Glembocki, B. V. Shanabrook, and W. T. Beard, Surf. Sci. **174**, 206 (1986).
 - ²⁸ S. Selci, A. Cricenti, M. Righini, C. Petrillo, F. Sacchetti, F. Alexandre, and G. Chiarotti, Solid State Commun. **79**, 561 (1991).
 - ²⁹ H. Quiang, F. H. Pollak, C. M. Sotomayor Torres, W. Leitch, A. H. Kean, M. A. Stroschio, G. J. Iafrate, and K. W. Kim, Appl. Phys. Lett. **61**, 1411 (1992).
 - ³⁰ F. H. Pollak, in *Phonons in Semiconductor Nanostructures*, edited by J. P. Leburton *et al.* (Kluwer, Amsterdam, 1993), p. 341.
 - ³¹ N. T. Pelekanos, J. Ding, M. Hagerott, V. A. Nurmikko, H. Luo, N. Samarth, and J. K. Furdyna, Phys. Rev. B **45**, 6037 (1992).
 - ³² Y. Chen, G. P. Kothiyal, J. Singh, and P. K. Battacharya, Superlatt. Microstruct. **3**, 657 (1987).
 - ³³ V. Srinivas, J. Hryniewicz, Y. J. Chen, and C. E. C. Wood, Phys. Rev. B **46**, 10 193 (1992).
 - ³⁴ J. P. Doran, J. F. Donegan, J. Hegarty, R. D. Feldman, and R. F. Austin, Solid State Commun. **81**, 801 (1992).
 - ³⁵ L. Schultheis, A. Honold, J. Kuhl, K. Köhler, and C. W. Tu, Phys. Rev. B **34**, 9027 (1986).
 - ³⁶ J. Kuhl, A. Honold, L. Schultheis, and C. W. Tu, in *Festkörperprobleme*, Vol. 29 of *Advances in Solid State Physics* (Vieweg, Braunschweig, 1989), p. 157.
 - ³⁷ J. Feldmann, G. Peter, E. O. Göbel, P. Dawson, K. Moore, C. Foxon, and R. J. Elliott, Phys. Rev. Lett. **59**, 2337 (1987).
 - ³⁸ V. L. Alperovich, V. M. Zaletin, A. F. Kravchenko, and A. S. Terekhov, Phys. Status Solidi B **77**, 465 (1976).
 - ³⁹ D. A. B. Miller, D. S. Chemla, D. J. Eilenberger, P. W. Smith, A. C. Gossard, and W. T. Tsang, Appl. Phys. Lett. **41**, 679 (1982).
 - ⁴⁰ J. Humlíček, E. Schmidt, L. Bočánek, R. Švehla, and K. Ploog, Phys. Rev. B **48**, 5241 (1993).
 - ⁴¹ T. L. Reinecke (private communication) and (unpublished).
 - ⁴² T. Hiroshima, Solid State Commun. **68**, 483 (1988).
 - ⁴³ K. T. Tsen, K. R. Wald, T. Ruf, P. Y. Yu, and H. Morkoç, Phys. Rev. Lett. **67**, 2557 (1991).
 - ⁴⁴ P. Lawaetz, Phys. Rev. **174**, 867 (1968).
 - ⁴⁵ D. D. Nolte, W. Walukiewicz, and E. E. Haller, Phys. Rev. Lett. **59**, 501 (1987).
 - ⁴⁶ *Physics of Group IV Elements and III-V Compounds*, edited by O. Madelung, M. Schulz, and H. Weiss, Landolt-Börnstein, Vol. 17a (Springer-Verlag, Berlin, 1982).
 - ⁴⁷ A similar approach has been used in the evaluation of isotopic disorder effects on phonon linewidths in H. D. Fuchs, C. H. Grein, C. Thomsen, M. Cardona, W. L. Hansen, E. E. Haller, and K. Itoh, Phys. Rev. B **43**, 4835 (1991).